Pneumatospinning Biomimetic Scaffolds for Meniscus Tissue Engineering

Erik W. Dorthé[1], Austin B. Williams[2], Shawn P. Grogan[1] and Darryl D. D'Lima[1]*

[1]Department of Orthopaedics, Shiley Center for Orthopaedic Research and Education, Scripps Health, San Diego, CA, United States, [2]Intitute for Biomedical Sciences, San Diego, CA, United States

Nanofibrous scaffolds fabricated via electrospinning have been proposed for meniscus tissue regeneration. However, the electrospinning process is slow, and can only generate scaffolds of limited thickness with densely packed fibers, which limits cell distribution within the scaffold. In this study, we explored whether pneumatospinning could produce thicker collagen type I fibrous scaffolds with higher porosity, that can support cell infiltration and neo-fibrocartilage tissue formation for meniscus tissue engineering. We pneumatospun scaffolds with solutions of collagen type I with thicknesses of approximately 1 mm in 2 h. Scanning electron microscopy revealed a mix of fiber sizes with diameters ranging from 1 to 30 µm. The collagen scaffold porosity was approximately 48% with pores ranging from 7.4 to 100.7 µm. The elastic modulus of glutaraldehyde crosslinked collagen scaffolds was approximately 45 MPa, when dry, which reduced after hydration to 0.1 MPa. Mesenchymal stem cells obtained from the infrapatellar fat pad were seeded in the scaffold with high viability (>70%). Scaffolds seeded with adipose-derived stem cells and cultured for 3 weeks exhibited a fibrocartilage meniscus-like phenotype (expressing COL1A1, COL2A1 and COMP). *Ex vivo* implantation in healthy bovine and arthritic human meniscal explants resulted in the development of fibrocartilage-like neotissues that integrated with the host tissue with deposition of glycosaminoglycans and collagens type I and II. Our proof-of-concept study indicates that pneumatospinning is a promising approach to produce thicker biomimetic scaffolds more efficiently that electrospinning, and with a porosity that supports cell growth and neo-tissue formation using a clinically relevant cell source.

Keywords: pneumatospinning, solution blow spinning, electrospinning, fibrous scaffolds, infra patella fat pad, meniscal tears, meniscal repair

INTRODUCTION

Menisci are an essential tissue in knee joints that contribute to load distribution, knee stability, and protect articular cartilage during normal activity. Injuries to menisci are common, with an estimated incidence between 600,000 and 850,000 in the United States alone, 90% of which require surgical intervention (Milachowski et al., 1989; DeHaven, 1999; Turman and Diduch, 2008). Tears occurring in the vascular zone have a higher rate of repair *via* surgery (Makris et al., 2011). Very few tears in the avascular zone heal, and around a third of repairs fail. Smaller tears are frequently repaired using sutures, screws, arrows or darts (Fillingham et al., 2017; Ardizzone et al., 2020). However, many tears are too complex or extensive to repair and thus most surgeries involve partial, subtotal or total

meniscectomy (Ford et al., 2005; Fetzer et al., 2009). Loss of meniscal tissue alters joint loading dynamics, leading to joint destabilization and finally a progression to osteoarthritis (OA) (Englund et al., 2001; Lohmander et al., 2007; Rai et al., 2020; Rodeo et al., 2020). To address large tears or for the replacement of menisci, meniscal substitutions have been proposed for partial and total meniscus replacement (Winkler et al., 2020).

Efforts towards engineering meniscus tissues typically combine cells (Angele et al., 2021) with a variety of diverse natural and synthetic scaffolds (Kwon et al., 2019; Li et al., 2021). However, a central feature that underlies the load bearing role of meniscus is the unique organization of collagen fibers, which is an essential requirement for a functional engineered meniscus. To this end, we, and other groups, have applied electrospinning (ES) to create nanofibrous scaffolds that emulate the meniscus collagen fibrillar matrix using natural and synthetic polymer (Grogan et al., 2020; Wang et al., 2021).

Examples of ES scaffolds explored for meniscus regeneration include synthetic polymers such as polylactic acid (PLA) (Baek et al., 2015), polycaprolactone (PCL) (Baker and Mauck, 2007; Ionescu et al., 2012; Gopinathan et al., 2015), natural polymers such as collagen (Baek et al., 2016, Baek et al., 2018), or combinations such as PCL and silk fibroin (Li et al., 2020), poly(lactic-co-glycolic) acid (PLGA) and gelatin (Li et al., 2016), or PLA and collagen (Baek et al., 2019). These electrospun scaffolds were biocompatible, supported attachment of a variety of cell types including meniscus fibroblasts (Kang et al., 2006; Martinek et al., 2006; Puetzer et al., 2015; Baek et al., 2020), various sources of MSC (Pak et al., 2014; Oda et al., 2015; Chew et al., 2017; Baek et al., 2018; Sasaki et al., 2018; Rothrauff et al., 2019) and synovial cells (Horie et al., 2009; Kondo et al., 2019; Sekiya et al., 2019), and lead to neo-tissue formation and repair of *ex vivo* meniscal tears (Baek et al., 2016; Baek et al., 2019). Electrospun scaffolds show promise in terms of cytocompatibility and neotissue formation, however, electrospinning often requires days to generate a scaffold of even a few millimeters in thickness (Dos Santos et al., 2020). Layering of ES scaffolds (Baek et al., 2015; Fisher et al., 2015) or incorporating ES collagen micro/nanofibers within a macroporous PLA/PLGA foam have been described (Bahcecioglu et al., 2014) to generate thicker constructs. However, the issue of delamination under loading remains a concern. Moreover, the highly dense nature of the fibers comprising the scaffold hinder efficient cell seeding and migration throughout the scaffold. To overcome this issue, strategies have been adopted to increase scaffold porosity by including water soluble sacrificial fibers (Baker et al., 2012; Shimomura et al., 2015), or by incorporating growth factors or chemoattractants within the scaffold to facilitate cell migration, support proliferation and tissue formation (Qu et al., 2017; Qu et al., 2019; Baek et al., 2019).

Solution blow spinning or pneumatospinning is an alternate method of generating fibrous scaffolds. Pressurized gas driven through an outer nozzle generates a stream of polymer solution fed through the inner nozzle of a coaxial system (Dos Santos et al., 2020). Pneumatospinning relies on gas pressure instead of an
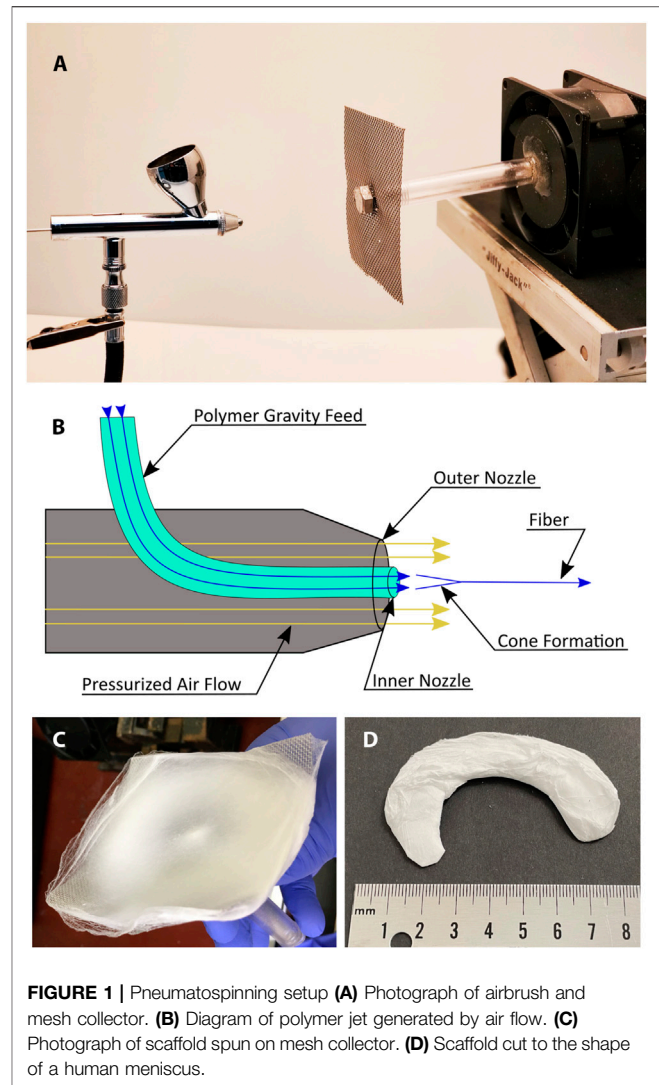

FIGURE 1 | Pneumatospinning setup **(A)** Photograph of airbrush and mesh collector. **(B)** Diagram of polymer jet generated by air flow. **(C)** Photograph of scaffold spun on mesh collector. **(D)** Scaffold cut to the shape of a human meniscus.

electric charge, which facilitates the fabrication of thicker constructs without the insulating effect that limits the thickness of electrospun constructs. Pneumatospinning is reportedly simpler, safer, more efficient, and can be achieved with less expensive and commercially available tools and therefore has the potential to overcome some of the limitations of electrospinning for meniscal repair (Behrens et al., 2014; Daristotle et al., 2016; Polk et al., 2018; Molde et al., 2020).

A wide range of materials have been pneumatospun to create nano- and microfibrous scaffolds. While pneumatospinning of synthetic polymers such as polyurethane (PU), polymethylmethacrylate, polyvinyl alcohol, PLA, and PCL is most commonly reported (Medeiros et al., 2009; Oliveira et al., 2011; Srinivasan et al., 2011; Behrens et al., 2014; Santos et al., 2016; Tomecka et al., 2017; Akentjew et al., 2019; Kopec et al., 2020); natural polymers such as silk fibroin and collagen have also been successfully pneumatospun (Magaz et al., 2018; Polk et al., 2018).

We therefore explored the potential of pneumatospinning for rapid generation of microfibrous collagen scaffolds seeded with human infrapatellar fat pad progenitors (IPFP-MSC) to facilitate meniscogenesis. We characterized scaffold microstructure, mechanical properties, and cytocompatibility. We analyzed cell migration and distribution, neotissue formation, and assessed proof of concept in the repair of meniscal tears in *ex vivo* bovine and human osteoarthritic menisci.

MATERIALS AND METHODS

Pneumatospinning System

Collagen type I (Semed S, generously supplied by DSM Biomedical, Exton, PA) was dissolved in hexafluoroisopropanol (HFIP) at concentrations between 5 and 10% wt/vol to establish the optimal concentration for spinning. The collagen solution was loaded into a customized gravity feed airbrush with a 350 μm nozzle (Anest Iwata, Yokohama) modified to run continuously. The airbrush consisted of an inner feed line, fed by gravity, leading to a nozzle and an outer air line, ending in a cap to form a coaxial outlet with the nozzle (**Figure 1**). The low pressure created by the escaping air drew solution from the inner nozzle. Air pressure on the air brush was set to 30 psi.

The target was a square section of flat stainless-steel mesh with a .03 cm wire diameter (TWP Inc., Berkeley) mounted on an electric motor and rotated at 650 RPM with the axis of rotation co-linear with the axis of the airbrush nozzle. The distance between the nozzle and target was set to 12 cm (**Figure 1**). The shape of the target mesh was varied by introducing 3-dimensional curvatures to assess potential for spinning a net meniscal shape (**Supplementary Figure S1**).

For comparison with electrospinning, scaffolds were fabricated as previously reported (Baek et al., 2016). Briefly, a collagen solution of 20% wt/vol was extruded toward a rotating drum with a potential difference of 18 kV.

Glutaraldehyde Crosslinking of Collagen Scaffolds

Collagen scaffolds were subjected to glutaraldehyde (GA, 25%, Thermo Fisher Scientific, Waltham, MA) vapor to induce crosslinking. We had previously used glutaraldehyde (GA) for electrospun collagen and found this to be an effective means of crosslinking collagen scaffolds (Baek et al., 2016; Baek et al., 2018). Collagen scaffolds on the collector mesh were suspended over an open beaker containing 30 ml GA solution and enclosed in a glass container for 48 h to contain the GA fumes in a chemical fume cabinet at 40°C. After GA crosslinking, scaffolds were cut to size and washed in PBS four to five times and stored in PBS at 4°C.

Mechanical Properties

Specimens were tested for tensile strength and tensile modulus using an Instron 8511 servohydraulic testing machine (Instron, Norwood, MA). Briefly, rectangular sections of 8 mm by 26 mm

($n = 5$) were cut from dry pneumatospun mats with the long axis tangent to the rotation of the collector (circumferentially oriented) or the long axis radial to the rotation of the collector (radially oriented, **Figure 2**). To test the effect of hydration, specimens were hydrated in 1x PBS for 1 h before mechanical testing ($n = 6$). The thickness and width of each specimen was measured with a digital caliper immediately prior to mechanical testing. Gauge length was measured for each specimen after mounting in the tensile grips. Specimens were mounted with a set of Instron grips and loaded to failure under tension at 4.2 mm/s. Load and displacement were recorded throughout the loading process.

Scanning Electron Microscopy (SEM)

For SEM, scaffolds were coated with 3.7 nm of Iridium and imaged on a Hitachi S-4800 SEM at 3 kV and 8 mm WD. SEM images were assessed for porosity and fiber morphology using ImageJ software (NIH, Bethesda, MD). Porosity was measured using ASTM F1854-15 (ASTM, 2015). Briefly, images were segmented to separate foreground fibers from background. Four lines were drawn horizontally across the image and values were measured along the corresponding profile. The percentage of pore space along these profiles was averaged to arrive at a value for the image. Pore size was measured across the longest axis of the pores to calculate average pore size in the transverse plane.

Cell Harvesting and Culture

Infrapatellar fat pad (IPFP) tissue was obtained from patients (74 year old female and 75 year old male) undergoing total knee replacement (approved by Scripps Institutional Review Board). Mesenchymal stem cells (IPFP-MSC) were isolated using a previously described method (Grogan et al., 2020). Briefly, IPFP tissues were minced using a scalpel to create fragments (~5 mm^3), which were placed into 6-well plate wells precoated with human collagen type I (Cell Adhere, StemCell Technologies, Vancouver, Canada). For the first 12 h, the tissue fragments were maintained in a CO_2 incubator at 37°C in only .5 ml MSC-medium (LONZA, Walkersville, MD) supplemented with Fibroblast Growth Factor 2 (FGF-2) (10 ng/ml; PeproTech, RockyHill, NJ). After 12 h, 1.5 ml of medium was added and the tissue fragments were cultured for 1–2 weeks until emergence of cells from the tissue. The remaining tissue fragments were discarded, and the emerging cells were detached using Accutase (Innovative Cell Technologies, Inc. San Diego, CA) and reseeded into collagen coated flasks at a density of 350,000 cells per cm^2.

Scaffold Cell Seeding and Culture Conditions

Pneumatospun and GA cross-linked collagen scaffolds were cut into rectangular specimens (approx. 1 cm by .5 cm) and washed in PBS extensively (at least 5 times in 5 ml PBS over 24 h). These scaffolds were seeded with IPFP-MSC (.5 × 10^6 cells per scaffold specimen), cultured in MSC medium, and placed upon an orbital shaker at 100 RPM (Ohaus Parsippany, NJ) in a CO_2 incubator at 37°C. The seeded scaffolds were maintained in MSC medium for

3–4 days for initial cell proliferation before changing to differentiation medium that consisted of Dulbecco's Modified Eagle Medium (DMEM) (Mediatech Inc., Manassas, VA), 1x ITS+1 supplement (Sigma-Aldrich, St. Louis, MO), 100 nM Dexamethasone (Sigma), 1.25 mg/ml human serum albumin (Bayer, Leverkusen, Germany), 100 μM ascorbic acid 2-phospahate (Sigma), 1% penicillin/streptomycin/gentamycin (PSG, Gibco, Carlsbad, CA) and supplemented with 10 ng/ml TGFβ3 (PeproTech, Rocky Hill, NJ). Scaffolds were cultured for 3 weeks (with medium changes every 3–4 days) to assess cell attachment, viability, and gene expression.

Cell Viability Assessments

A total of 11 seeded scaffolds were used to assess viability using two different donors after 21 days in culture. Cell viability and distribution after 24 h or following 3 weeks in culture was measured with the Live/Dead kit (Invitrogen, Waltham, MA). The staining buffer consisted of Ethidium Homodimer-1 (8 mM) and Calcein-AM (1.6 mM) suspended in PBS. The cell seeded collagen scaffolds were incubated for 30–40 min before visualization with either a fluorescence microscope (Axiovert 200M, Zeiss, Jena, Germany) or via a confocal laser microscope (LSM-810; Zeiss). Image processing by thresholding and segmentation was used to remove the background scaffold stain (**Supplementary Figure S2**). The percentage of live and dead cells was calculated using ImageJ/Fiji (Rueden et al., 2017).

Ex vivo Meniscus Repair Models

Bovine explants: Whole bovine knees with the knee capsule intact were obtained from Animal Technologies, Inc. (Tyler, TX). Meniscal tissue explants of approximately 1 cm wide and x 3 cm deep were cut under sterile conditions. Explants were cultured in DMEM with 10% CS and 1% PSG until ready to use.

Human explants: Menisci were obtained from four patients (69.3 ± 10.1 years, three female, one male) following total knee arthroplasty (approved by Scripps Institutional Review Board). The menisci were cut into tissue explants of around 1 cm × 1 cm and each cultured in DMEM with 10% CS and 1% PSG until ready for scaffold implantation (within 2 days).

Collagen scaffolds (approx. 1 cm long, .5 cm wide, and .2 cm thick) were seeded with IPFP-MSC (.5 × 10⁶ per scaffold) and cultured for 3 days in MSC-medium, followed by 7 days in differentiation medium. Scaffolds (n = 29) were implanted to repair surgically created longitudinal or transverse defects in human (n = 4 human donors, n = 17 explants) and bovine explants (n = 2 knees, n = 12 explants). The longitudinal defects were created in the red-white region and the transverse defects spanned the red-white regions. The implanted scaffolds and explant tissue was cultured for 3 weeks in the differentiation medium, with changes every 3–4 days. At the end of culture, the explants were fixed and processed for paraffin embedding and subsequent histological analyses.

Histology and Immunohistochemistry

Paraffin embedded sections (4 μm thick) were mounted on glass slides for staining with Safranin O-fast green or immunohistochemistry for collagen types I and II as previously described (van Schaik et al., 2021). Briefly, paraffin cut sections were deparaffinized and treated with pepsin for 9 min at 37°C in a humidified chamber (Digest-All 3, Thermo Fisher Scientific). Rabbit anti-human collagen type I antibody (1 μg/ml; Ab 34,710, Abcam, Cambridge, MA) and mouse anti-human collagen type II (2 μg/ml; II-II6B3, Hybridoma Bank, University of Iowa) was used as the primary antibodies, which were incubated at 4°C for 12–16 h in a humid chamber. The ImmPRESS secondary DAB (Brown) or AP (red) kits were used for color development (Vector Laboratories, Burlingame, CA). Non-specific staining was evaluated using species-matched isotype controls at the same concentration as the specific primary antibodies.

Gene Expression

Following the manufacturer's instructions (Qiagen, Valencia, CA), scaffolds were minced by scalpel in RLT buffer and then subjected to homogenization using the Qiashredder. Total RNA was extracted using the RNeasy kit (Qiagen) and cDNA was made using the High Capacity cDNA Reverse Transcription Kit (Applied Biosystems, Foster City, California). Verified primer/probe assays were purchased from Applied Biosystems to monitor the expression levels of COL1A1, COL2A1, COMP, ACAN, and THY1 relative to the GAPDH (housekeeping gene). The gene expression levels of IPFP-MSC in monolayer culture were used to calculate relative changes in expression level following culture on the pneumatospun collagen scaffolds. Gene expression was normalized to GAPDH and we used the ΔCt method as previously reported (Martin et al., 2001).
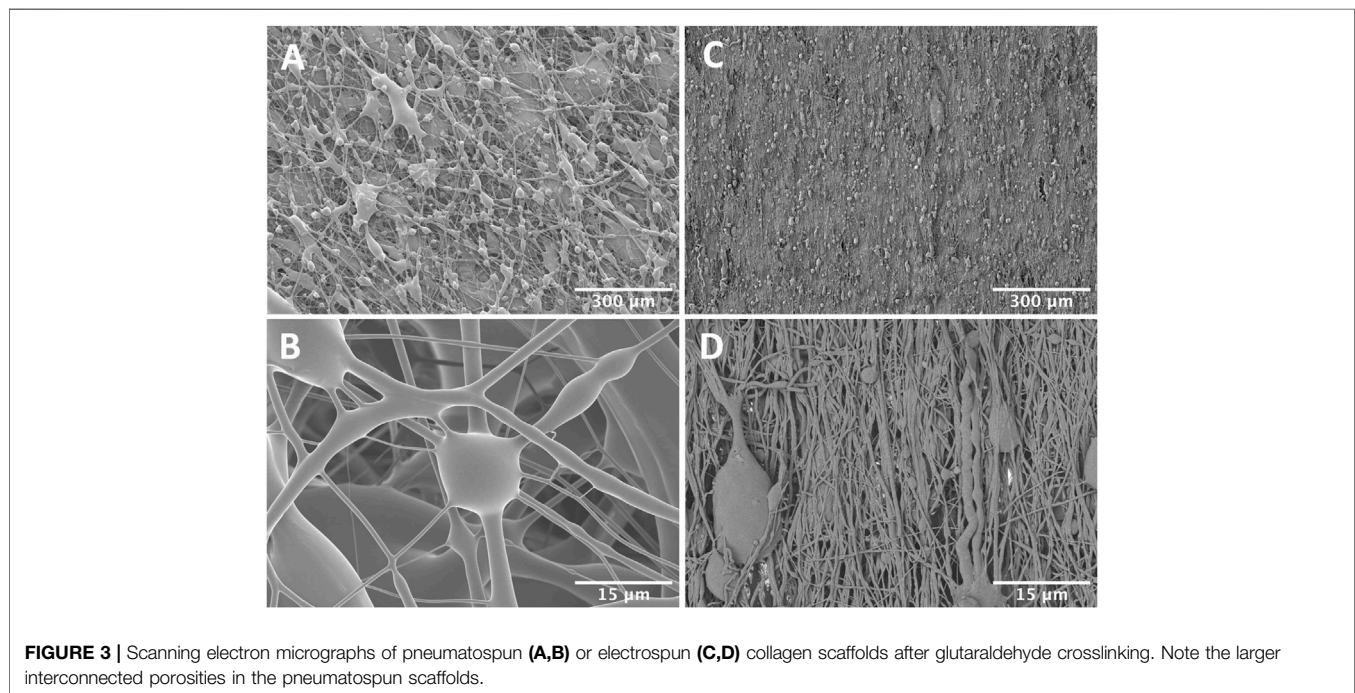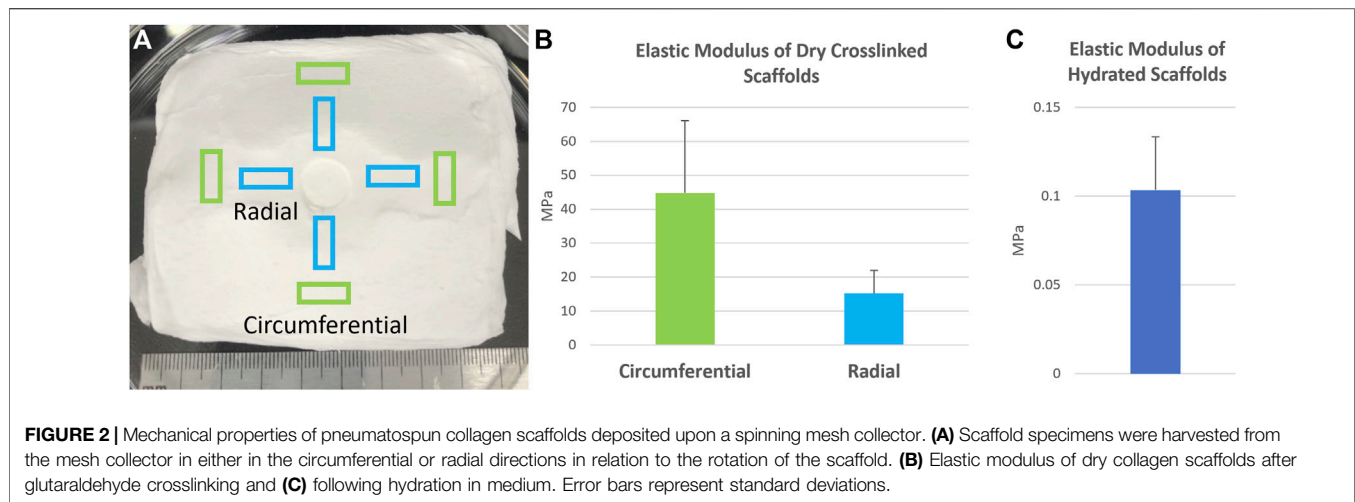
Statistical Analysis

Difference in gene expression between IPFP-MSC cultured on pneumatospun scaffolds and cells in monolayer cultures were tested for significance at $p < .05$, using the online BootstRatio application (http://regstattools.net/br) (Cleries et al., 2012).

RESULTS

Efficient Fabrication of Microfibrous Collagen Scaffolds

Pneumatospinning involves a gravity-fed airbrush which generated undesirable turbulence at traditional collector targets used in electrospinning such as flat plates or solid drums. We therefore selected meshed collectors that permit air flow through the target, reduce turbulence, and result in more consistent accumulation of spun fibers. To further reduce turbulence at the target, we mounted a fan behind a stationary collector to direct air through the target and mounted the target to the spinning fan to induce circumferential alignment of fibers.

We tested a range of collagen solution concentrations between 5 and 10% wt/vol to identify the optimal solution that could be reliably dispensed. Solutions below 6% formed insufficient fibers, while those above 9% tended to clog the nozzle of the airbrush. A 9% solution was chosen for all following experiments. 60 ml of collagen solution generated a 1 mm thick scaffold of collagen

FIGURE 2 | Mechanical properties of pneumatospun collagen scaffolds deposited upon a spinning mesh collector. **(A)** Scaffold specimens were harvested from the mesh collector in either the circumferential or radial directions in relation to the rotation of the scaffold. **(B)** Elastic modulus of dry collagen scaffolds after glutaraldehyde crosslinking and **(C)** following hydration in medium. Error bars represent standard deviations.

FIGURE 3 | Scanning electron micrographs of pneumatospun **(A,B)** or electrospun **(C,D)** collagen scaffolds after glutaraldehyde crosslinking. Note the larger interconnected porosities in the pneumatospun scaffolds.

fibers in less than 2 h. This was significantly faster than our electrospinning experiments which required over 24 h to generate 250 μm thick scaffolds.

We also demonstrated the potential to create scaffolds of varying shapes, using curved targets with radial ripples (**Supplementary Figure S1**). Glutaraldehyde crosslinked mats spun onto these targets retained the curvature of the targets after removal, but showed no appreciable variation in thickness. For subsequent experiments in this study, we used flat square mesh collectors.

Scaffold Properties
Before crosslinking, spun collagen mats were fragile, fragmented upon removed from the target substrate, and dissolved in culture.

After glutaraldehyde crosslinking, collagen mats could be easily removed intact from the target. By 3 weeks, cultured scaffolds swelled and softened, but retained their net spun shape and could be easily manipulated with forceps for loading into mechanical testing fixtures or for surgical implantation in *ex vivo* tissue samples.

Dry collagen GA crosslinked scaffolds exhibited an elastic modulus of around 45 MPa, which was reduced significantly after hydration to .1 ± .03 MPa (**Figure 2**). Dry scaffolds failed consistently within the gauge length of the test setup, while hydrated scaffolds tended to fail near the tissue grips. SEM imaging of the GA crosslinked pneumatospun scaffolds revealed a heterogenous distribution of fiber sizes and large, interconnected porosities (**Figure 3**). This contrasted with aligned, electrospun
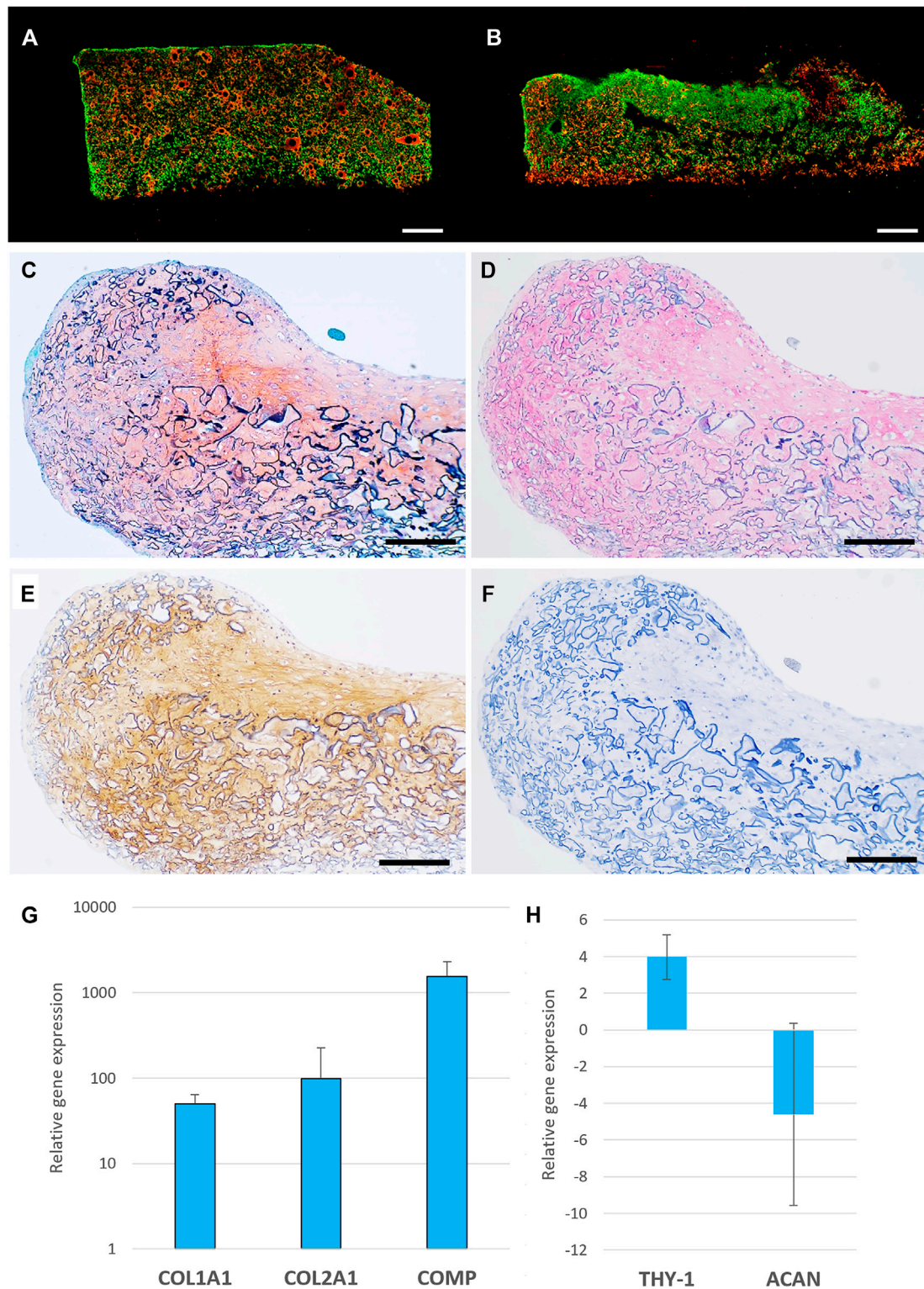
FIGURE 4 | Cell viability, histology and gene expression of IPFP-MSC seeded pneumatospun collagen scaffolds. **(A,B)** Cell viability of IPFP-MSC seeded collagen scaffolds (live cells = green), dead cells = red, bar = 1000 μm) **(C)** Safranin O stain of neotissue formed on collagen scaffold. **(D)** Collagen type I immunostaining (AP red). **(E)** Collagen type II immunostaining (DAB brown). **(F)** Isotype control immunostaining. (Bar = 200 μm) **(G,H)**. Gene expression levels of IPFP-MSC seeded on collagen scaffolds after 3 weeks in serum free medium relative to monolayer undifferentiated cultured IPFP-MSC (n = 6).
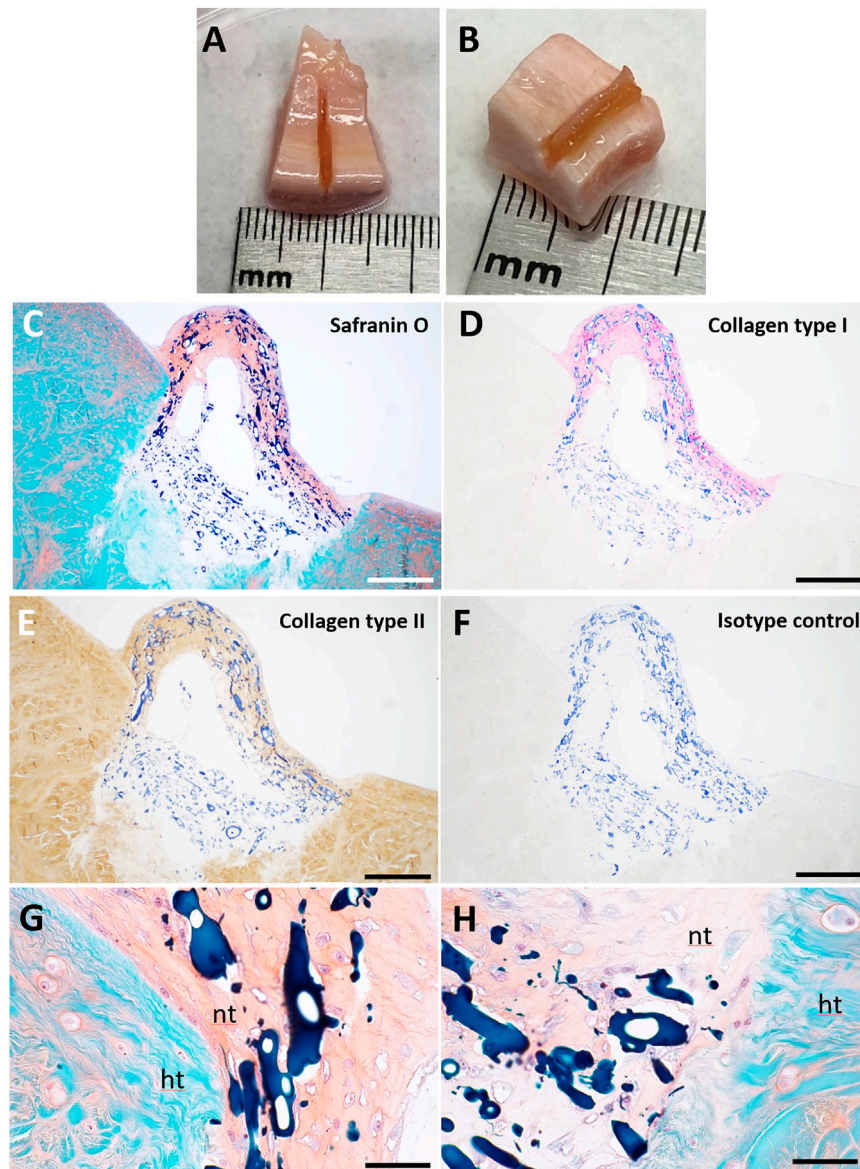
FIGURE 5 | Pneumatospun collagen scaffolds seeded with human IPFP cells and implanted into *ex vivo* bovine meniscus and culture for 3 weeks. **(A,B)** Photographs of implanted collagen scaffolds. **(C)** Safranin O staining. **(D)** Collagen type I immunostaining. **(E)** Collagen type II immunostaining. **(F)** Isotype control. **(G,H)** Higher magnification of Safranin O stained image showing integration of neotissue (nt) with host tissue (ht). The collagen scaffold is stained dark blue. (C-F Bar = 200 μm; G-H Bar = 50 μm).

scaffolds which have low porosity and more uniform, nanoscale fibers (**Figure 3**). Pneumatospun fibers appeared irregular with diameters ranging from 1 to 30 μm. The overall porosity of the collagen scaffold in the transverse plane was approximately 48% with pore sizes ranging from 7.4 to 100.7 μm with a median of 23.8 μm and a mean of 25.7 μm. We also observed bead formation which is related to the surface tension of the solution and can be reduced by optimizing solution and spinning parameters.

Neotissue Formation

Glutaraldehyde crosslinked pneumatospun collagen scaffolds were seeded with IPFP-MSC, cultured in 6-well plates in MSC medium and placed on an orbital shaker overnight in the incubator. This approach enhanced cell attachment and infiltration into the scaffold (**Supplementary Figure S3**). After 3 weeks of culture in serum-free differentiation medium, IPFP-MSC were observed throughout the pneumatospun collagen scaffolds with 70.2 ± 7.5% viability (**Figures 4A,B**).

On histological analysis, IPFP-MSC seeded into the scaffolds generated a fibrocartilage-like neotissue with extracellular matrix containing glycosaminoglycans (Safranin O positive; **Figure 4C**), collagen types I and II (**Figures 4D–F**). This histology was generally consistent with the gene expression profile of
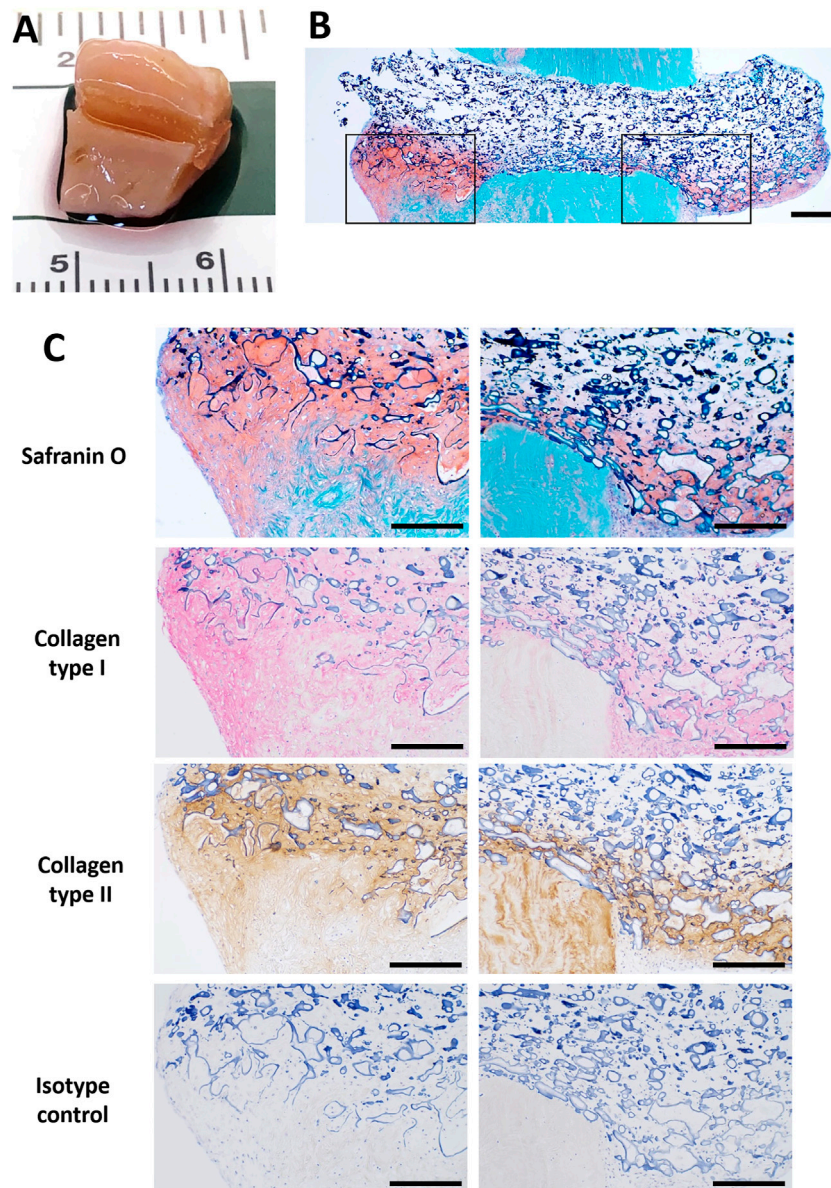
FIGURE 6 | Pneumatospun collagen scaffolds seeded with human IPFP cells and implanted into human OA meniscus explant (72 year-old female) and cultured for 3 weeks. **(A)** Photograph of implanted scaffold. **(B)** Overview of section stained with Safranin O showing neotissue development in meniscus defect (bar = 500 μm). **(C)** Histologic images of sections stained with Safranin O and immunostained with collagen type I (AP red), collagen type II (DAB brown), and isotype control regions of inset regions outlined in **(B)** (bar = 300 μm).

increased COL1A1, COL2A1 and COMP, THY-1 (CD90) and reduced ACAN expression compared to IPFP-MSC in monolayer culture (**Figures 4G,H**).

Repair of Ex Vivo Meniscus Tears

We assessed potential for repair of meniscus tears by implanting scaffolds seeded with IPFP-MSC into surgically created defects in normal healthy bovine meniscus (**Figures 5A,B**) or in osteoarthritic human meniscus resected from patients that had undergone TKA (**Figure 6A**). After 3 weeks of culture in differentiation medium, neo-fibrocartilaginous tissue developed in the bovine meniscus that integrated with the host tissue (**Figure 5**). More GAG deposition was noted in the superficial region corresponding spatially with the GAG seen in the host tissue (**Figure 5C**). The mix of collagen types I and II indicated a fibrocartilage-like composition. Cell-seeded collagen scaffolds implanted into osteoarthritic human menisci (**Figure 6A**) also resulted in similar fibrocartilage-like neotissue which integrated with host tissue with a positive Safranin O and a collagen type I and II staining profile (**Figures 6B,C**).

DISCUSSION

We explored pneumatospinning to fabricate microfibrous collagen scaffolds as a more efficient approach to electrospinning (ES) for meniscal tissue engineering, with potential for greater porosity to facilitate cell seeding and migration, generation of meniscus-like tissue, and to repair meniscal tears. We demonstrated that pneumatospinning can rapidly produce scaffolds with a spectrum of micron-sized fibers and appropriate porosity. Pneumatospun collagen scaffolds were biocompatible, and permitted rapid IPFP-MSC attachment and colonization, and formation of neo-fibrocartilage meniscus-like tissue, especially when implanted into healthy bovine or osteoarthritic human meniscus explants.

Several synthetic polymers (polymethylmethacrylate, polylactic acid, and polystyrene) have been pneumatospun to produce micro- and nano-fibers up to 100x faster than electrospinning) (Medeiros et al., 2009). The authors found that electrospinning typically dispensed solutions between 4 and 10 µl/min while pneumatospinning dispensing rates can be increased up to 200 µl/min without altering fiber diameter (Medeiros et al., 2009). Most other studies did not report on the final thickness of the deposited scaffold or the accumulation rate over a given time. However, pneumatospun fiber mats are reported to take a few seconds to minutes to build a mat of significant thickness with deposition rates of .1 ml/min or more (Medeiros et al., 2009; Oliveira et al., 2011; Behrens et al., 2016). Others have reported pneumatospun mat thickness ranging from 130 µm to 1 mm (Behrens et al., 2016; Kopec et al., 2020; Molde et al., 2020). Polk et al. (2018) rapidly pneumatospun 200 µm thick collagen type I scaffolds in 5 min, which was 32x faster than electrospun scaffolds. To our knowledge, this is the first study reporting on pneumatospinning for fabricating scaffolds for meniscus regeneration. We generated scaffolds at approximately .5 mm in thickness/hr, which was significantly more efficient than our previous reports on electrospinning which required over 24 h to produce a .25 mm thick electrospun scaffold (Baek et al., 2016); equivalent to a 50x increase in fiber deposition rate.

Pneumatospinning can generate fibers with diameters ranging from 70 nm to as large as 100 µm (Sinha-Ray et al., 2015; Daristotle et al., 2016; Dos Santos et al., 2020) by tuning process variables such as the polymer injection rate and concentration, temperature, air/gas pressure and nozzle geometry (Sinha-Ray et al., 2015; Medeiros et al., 2016; Dos Santos et al., 2020). We pneumatospun collagen fibers ranging from 1 to 30 µm, which were larger than our previous studies with ES collagen fiber (250–860 nm) (Baek et al., 2016). Our pneumatospun collagen fiber diameters were also larger than the average fiber diameter of 224 nm reported for pneumatospun type I atelocollagen scaffolds (Polk et al., 2018). This difference in fiber diameters could be attributed to differences in collagen (atelocollagen vs. soluble collagen), collagen concentration (40 vs. 9%), solvent (acetic acid vs. HFIP), air pressure (60 psi vs. 30 psi), and collector properties.

Electrospinning typically generates densely packed nanofibrous mats with low porosity which can inhibit cell migration into the scaffolds (Baker et al., 2008). Modifications such as sacrificial fibers or microparticles of polyethylene oxide are required to increase porosity and enhance cell infiltration (Baker et al., 2008; Wang et al., 2013). One advantage of our pneumatospun scaffolds was the inherent increased porosity which enhances potential for cell migration. We noted a porosity of nearly 50% in our scaffolds (with pore sizes averaging 26 µm) which supported cell migration. Others have reported varying pore sizes with pneumatospun materials, ranging from 3 to 6 µm for PU (Kopec et al., 2020); 10–50 µm with E1001 (1 k), a tyrosine-derived polycarbonate (Molde et al., 2020); and 25 µm to over 100 µm for scaffolds of PLA and dimethyl carbonate (Medeiros et al., 2016).

Fiber alignment replicating the microstructure of meniscal tissue is important to engineer tissue with biomimetic properties. We used a rotating mesh collector to direct circumferential fiber alignment. Although, SEM did not reveal differences in alignment of fibers, crosslinked collagen scaffold samples in the circumferential direction were three times stiffer in comparison to samples in the radial direction (15 KPa) from the same scaffold. Increasing the speed of collector rotation or modifying collector shape may enhance fiber alignment (Baek et al., 2015; Baek et al., 2016; Baek et al., 2018). For example, a funnel between the nozzle and the collector has been effective in channeling airflow and aligning in-flight fibers (Magaz et al., 2018); and a cylindrical tube with internal spokes collected aligned pneumatospun fibers (Polk et al., 2018).

The meniscus is composed of a fibrocartilaginous tissue that displays variations in the distribution of ECM molecules particularly collagens type I and II, and GAGs (Makris et al., 2011; Murphy et al., 2019). In our study, seeding IPFP-MSC upon pneumatospun collagen scaffolds increased expression of COL1A1, COL2A1, COMP and THY-1 (CD90). COMP plays a critical role in mediating various ECM component interactions such as fibronectin, many collagens (types I, II IX, XII, and XIV) and proteoglycans such as aggrecan, chondroitin sulfates, and heparan sulfate (Chen et al., 2007; Acharya et al., 2014). The increased gene expression of THY-1 also corresponds with a fibrocartilaginous phenotype (Grogan et al., 2017; Grogan et al., 2018). These increases in meniscogenic gene expression were reflected in development of fibrocartilaginous-like neotissue with distinct collagen type I and II protein deposition in a matrix containing GAGs.

Ex vivo meniscus tissue cultures are increasingly being utilized as models to assess *in vitro* repair and regeneration (Cucchiarini et al., 2009; Cucchiarini et al., 2015; Marrella et al., 2018; Resmi et al., 2020). We previously characterized an *ex vivo* meniscus explant model of longitudinal tears repaired with collagen ES scaffolds seeded with human meniscus cells (Baek et al., 2016; Baek et al., 2019) and documented composition of neotissue and integration with host explant. In the present study, implantation of thicker pneumatospun scaffolds seeded with IPFP-MSC into meniscal defects resulted in fibrocartilaginous tissues composed of GAGs and collagen types I and II. The scaffolds used in this study may therefore be more suitable for supporting the development of avascular meniscus-like tissues, that typically

contain higher concentrations of collagen type II and GAGs than the vascular meniscus regions.

Despite the promising results with pneumatospun collagen scaffolds, there are limitations to overcome. Hydration of glutaraldehyde crosslinked collagen scaffolds in culture significantly decreased mechanical properties, reducing its potential for broader clinical applications such as meniscus replacement. Incorporation of artificial polymers, such as PLA, may increase the mechanical properties as we and others have previously demonstrated with coaxial electrospun fibers (Tong et al., 2015; Singh et al., 2018; Baek et al., 2019; Baek et al., 2020). Our nozzle to collector arrangement did generate encouraging differences in mechanical properties based on sample orientation but did not result in visible fiber alignment; and alternate approaches need to be explored. Our *in vitro* and *ex vivo* systems provided proof of concept of cytocompatibility, cell distributions neo-tissue formation. However, *in vivo* experiments are needed to validate suitability of translation of tissue engineered scaffolds for meniscus repair.

CONCLUSION

Pneumatospinning is a promising approach to rapidly generate collagen fibers for meniscus tissue engineering with significantly greater efficiency of scaffold fabrication than electrospinning. The increased porosity effectively supported IPFP-derived cell colonization and differentiation. The resultant neo-fibrocartilage tissue integrated into normal bovine and arthritic human menisci defects. For translation to clinical applications, enhanced mechanical properties and validation in clinically relevant meniscal repair and regeneration models are required.

DATA AVAILABILITY STATEMENT

The original contributions presented in the study are included in the article/**Supplementary Material**, further inquiries can be directed to the corresponding author.

ETHICS STATEMENT

The studies involving human participants were reviewed and approved by Scripps Institutional Review Board. The patients/participants provided their written informed consent to participate in this study.

REFERENCES

Acharya, C., Yik, J. H. N., Kishore, A., Van Dinh, V., Di Cesare, P. E., and Haudenschild, D. R. (2014). Cartilage Oligomeric Matrix Protein and its Binding Partners in the Cartilage Extracellular Matrix: Interaction, Regulation and Role in Chondrogenesis. *Matrix Biol.* 37, 102–111. doi:10.1016/j.matbio.2014.06.001

Akentjew, T. L., Terraza, C., Suazo, C., Maksimcuka, J., Wilkens, C. A., Vargas, F., et al. (2019). Rapid Fabrication of Reinforced and Cell-Laden Vascular Grafts

AUTHOR CONTRIBUTIONS

ED, AW, SG, and DD'D were responsible for the overall experimental design. ED, SG, and DD'D wrote the manuscript in close collaboration with the other authors. ED and AW designed and conducted the pneumatospinning and electrospinning. SG coordinated cell culture studies, RT-PCR and histology. ED, AW, and DD'D designed and performed mechanical tests. All authors discussed the results and approved the final version of the article.

FUNDING

ACKNOWLEDGMENTS

SUPPLEMENTARY MATERIAL

The Supplementary Material for this article can be found online at: https://www.frontiersin.org/articles/10.3389/fbioe.2022.810705/full#supplementary-material

Supplementary Figure S1 | Photographs of different collector shapes. **(A)** Flat mesh **(B)** Curved mesh **(C,D)** 3D curved shapes.

Supplementary Figure S2 | Cell viability of IPFP-MSC seeded pneumatospun collagen scaffolds after overnight incubation on orbital shaker. **(A)** Live cells (green) and **(B)** dead cells (red) (Magnification 10x).

Supplementary Figure S3 | ImageJ was used for image processing to remove background staining and extract green (live/cytoplasm) and dead (red /nuclei) cells for viability assessments. **(A)** Confocal microscopy image; **(B)** Live cells labeled green (cell count = 13,773); **(C)** Dead cells labeled red (cell count = 1201): cell viability = 92% (bar = 1000 μm).

Supplementary Figure S4 | Immunohistochemistry for collagen types I and II. Left column: Negative isotype controls; Right column: positive stains. **(A,B)** Type I collagen stain for bovine meniscus; **(C,D)** Type I collagen stain for human meniscus; **(E,F)** Type II collagen stain for human articular cartilage.

Structurally Inspired by Human Coronary Arteries. *Nat. Commun.* 10 (1), 3098. doi:10.1038/s41467-019-11090-3

Angele, P., Docheva, D., Pattappa, G., and Zellner, J. (2021). Cell-based Treatment Options Facilitate Regeneration of Cartilage, Ligaments and Meniscus in Demanding Conditions of the Knee by a Whole Joint Approach. *Knee Surg. Sports Traumatol. Arthrosc.* doi:10.1007/s00167-021-06497-9

Ardizzone, C. A., Houck, D. A., McCartney, D. W., Vidal, A. F., and Frank, R. M. (2020). All-Inside Repair of Bucket-Handle Meniscal Tears: Clinical Outcomes and Prognostic Factors. *Am. J. Sports Med.* 48 (13), 3386–3393. doi:10.1177/0363546520906141

ASTM (2015). *Standard Test Method for Stereological Evaluation of Porous Coatings on Medical Implants*. West Conshohocken, PA: ASTM International. Vol. ASTM F1854-15.

Baek, J., Chen, X., Sovani, S., Jin, S., Grogan, S. P., and D'Lima, D. D. (2015). Meniscus Tissue Engineering Using a Novel Combination of Electrospun Scaffolds and Human Meniscus Cells Embedded within an Extracellular Matrix Hydrogel. *J. Orthop. Res.* 33 (4), 572–583. doi:10.1002/jor.22802

Baek, J., Lee, E., Lotz, M. K., and D'Lima, D. D. (2020). Bioactive Proteins Delivery through Core-Shell Nanofibers for Meniscal Tissue Regeneration. *Nanomedicine: Nanotechnology, Biol. Med.* 23, 102090. doi:10.1016/j.nano.2019.102090

Baek, J., Lotz, M. K., and D'Lima, D. D. (2019). Core-Shell Nanofibrous Scaffolds for Repair of Meniscus Tears. *Tissue Eng. A* 25 (23-24), 1577–1590. doi:10.1089/ten.TEA.2018.0319

Baek, J., Sovani, S., Choi, W., Jin, S., Grogan, S. P., and D'Lima, D. D. (2018). Meniscal Tissue Engineering Using Aligned Collagen Fibrous Scaffolds: Comparison of Different Human Cell Sources. *Tissue Eng. Part A* 24 (1-2), 81–93. doi:10.1089/ten.TEA.2016.0205

Baek, J., Sovani, S., Glembotski, N. E., Du, J., Jin, S., Grogan, S. P., et al. (2016). Repair of Avascular Meniscus Tears with Electrospun Collagen Scaffolds Seeded with Human Cells. *Tissue Eng. Part A* 22 (5-6), 436–448. doi:10.1089/ten.TEA.2015.0284

Bahcecioglu, G., Buyuksungur, A., Kiziltay, A., Hasirci, N., and Hasirci, V. (2014). Construction and *In Vitro* Testing of a Multilayered, Tissue-Engineered Meniscus. *J. Bioactive Compatible Polym.* 29 (3), 235–253. doi:10.1177/0883911514529688

Baker, B. M., Gee, A. O., Metter, R. B., Nathan, A. S., Marklein, R. A., Burdick, J. A., et al. (2008). The Potential to Improve Cell Infiltration in Composite Fiber-Aligned Electrospun Scaffolds by the Selective Removal of Sacrificial Fibers. *Biomaterials* 29 (15), 2348–2358. doi:10.1016/j.biomaterials.2008.01.032

Baker, B. M., and Mauck, R. L. (2007). The Effect of Nanofiber Alignment on the Maturation of Engineered Meniscus Constructs. *Biomaterials* 28 (11), 1967–1977. doi:10.1016/j.biomaterials.2007.01.004

Baker, B. M., Shah, R. P., Silverstein, A. M., Esterhai, J. L., Burdick, J. A., and Mauck, R. L. (2012). Sacrificial Nanofibrous Composites Provide Instruction without Impediment and Enable Functional Tissue Formation. *Proc. Natl. Acad. Sci.* 109 (35), 14176–14181. doi:10.1073/pnas.1206962109

Behrens, A. M., Casey, B. J., Sikorski, M. J., Wu, K. L., Tutak, W., Sandler, A. D., et al. (2014). *In Situ* Deposition of PLGA Nanofibers via Solution Blow Spinning. *ACS Macro Lett.* 3 (3), 249–254. doi:10.1021/mz500049x

Behrens, A. M., Kim, J., Hotaling, N., Seppala, J. E., Kofinas, P., and Tutak, W. (2016). Rapid Fabrication of poly(DL-Lactide) Nanofiber Scaffolds with Tunable Degradation for Tissue Engineering Applications by Air-Brushing. *Biomed. Mater.* 11 (3), 035001. doi:10.1088/1748-6041/11/3/035001

Chen, F. H., Herndon, M. E., Patel, N., Hecht, J. T., Tuan, R. S., and Lawler, J. (2007). Interaction of Cartilage Oligomeric Matrix Protein/thrombospondin 5 with Aggrecan. *J. Biol. Chem.* 282 (34), 24591–24598. doi:10.1074/jbc.M611390200

Chew, E., Prakash, R., and Khan, W. (2017). Mesenchymal Stem Cells in Human Meniscal Regeneration: A Systematic Review. *Ann. Med. Surg.* 24, 3–7. doi:10.1016/j.amsu.2017.09.018

Clèries, R., Galvez, J., Espino, M., Ribes, J., Nunes, V., and de Heredia, M. L. (2012). BootstRatio: A Web-Based Statistical Analysis of Fold-Change in qPCR and RT-qPCR Data Using Resampling Methods. *Comput. Biol. Med.* 42 (4), 438–445. doi:10.1016/j.compbiomed.2011.12.012

Cucchiarini, M., Schetting, S., Terwilliger, E. F., Kohn, D., and Madry, H. (2009). rAAV-mediated Overexpression of FGF-2 Promotes Cell Proliferation, Survival, and α-SMA Expression in Human Meniscal Lesions. *Gene Ther.* 16 (11), 1363–1372. doi:10.1038/gt.2009.91

Cucchiarini, M., Schmidt, K., Frisch, J., Kohn, D., and Madry, H. (2015). Overexpression of TGF-β via rAAV-Mediated Gene Transfer Promotes the Healing of Human Meniscal Lesions *Ex Vivo* on Explanted Menisci. *Am. J. Sports Med.* 43 (5), 1197–1205. doi:10.1177/0363546514567063

Daristotle, J. L., Behrens, A. M., Sandler, A. D., and Kofinas, P. (2016). A Review of the Fundamental Principles and Applications of Solution Blow Spinning. *ACS Appl. Mater. Inter.* 8 (51), 34951–34963. doi:10.1021/acsami.6b12994

DeHaven, K. E. (1999). Meniscus Repair. *Am. J. Sports Med.* 27 (2), 242–250. doi:10.1177/03635465990270022301

Dos Santos, D. M., Correa, D. S., Medeiros, E. S., Oliveira, J. E., and Mattoso, L. H. C. (2020). Advances in Functional Polymer Nanofibers: From Spinning Fabrication Techniques to Recent Biomedical Applications. *ACS Appl. Mater. Inter.* 12 (41), 45673–45701. doi:10.1021/acsami.0c12410

Englund, M., Roos, E. M., Roos, H. P., and Lohmander, L. S. (2001). Patient-relevant Outcomes Fourteen Years after Meniscectomy: Influence of Type of Meniscal Tear and Size of Resection. *Rheumatology (Oxford)* 40 (6), 631–639. doi:10.1093/rheumatology/40.6.631

Fetzer, G., Spindler, K., Amendola, A., Andrish, J., Bergfeld, J., Dunn, W., et al. (2009). Potential Market for New Meniscus Repair Strategies -Evaluation of the MOON Cohort. *J. Knee Surg.* 22 (3), 180–186. doi:10.1055/s-0030-1247746

Fillingham, Y. A., Riboh, J. C., Erickson, B. J., Bach, B. R., Jr., and Yanke, A. B. (2017). Inside-Out versus All-Inside Repair of Isolated Meniscal Tears: An Updated Systematic Review. *Am. J. Sports Med.* 45 (1), 234–242. doi:10.1177/0363546516632504

Fisher, M. B., Henning, E. A., Söegaard, N., Bostrom, M., Esterhai, J. L., and Mauck, R. L. (2015). Engineering Meniscus Structure and Function via Multi-Layered Mesenchymal Stem Cell-Seeded Nanofibrous Scaffolds. *J. Biomech.* 48 (8), 1412–1419. doi:10.1016/j.jbiomech.2015.02.036

Ford, G. M., Hegmann, K. T., White, G. L., Jr., and Holmes, E. B. (2005). Associations of Body Mass index with Meniscal Tears. *Am. J. Prev. Med.* 28 (4), 364–368. doi:10.1016/j.amepre.2005.01.013

Gopinathan, J., Mano, S., Elakkiya, V., Pillai, M. M., Sahanand, K. S., Rai, B. K. D., et al. (2015). Biomolecule Incorporated Poly-ε-Caprolactone Nanofibrous Scaffolds for Enhanced Human Meniscal Cell Attachment and Proliferation. *RSC Adv.* 5 (90), 73552–73561. doi:10.1039/c5ra14315b

Grogan, S. P., Baek, J., and D'Lima, D. D. (2020). Meniscal Tissue Repair with Nanofibers: Future Perspectives. *Nanomedicine* 15 (25), 2517–2538. doi:10.2217/nnm-2020-0183

Grogan, S. P., Duffy, S. F., Pauli, C., Lotz, M. K., and D'Lima, D. D. (2018). Gene Expression Profiles of the Meniscus Avascular Phenotype: A Guide for Meniscus Tissue Engineering. *J. Orthop. Res.* 36 (7), 1947–1958. doi:10.1002/jor.23864

Grogan, S. P., Pauli, C., Lotz, M. K., and D'Lima, D. D. (2017). Relevance of Meniscal Cell Regional Phenotype to Tissue Engineering. *Connect. Tissue Res.* 58 (3-4), 259–270. doi:10.1080/03008207.2016.1268604

Horie, M., Sekiya, I., Muneta, T., Ichinose, S., Matsumoto, K., Saito, H., et al. (2009). Intra-articular Injected Synovial Stem Cells Differentiate into Meniscal Cells Directly and Promote Meniscal Regeneration without Mobilization to Distant Organs in Rat Massive Meniscal Defect. *Stem Cells* 27 (4), 878–887. doi:10.1634/stemcells.2008-0616

Ionescu, L. C., Lee, G. C., Huang, K. L., and Mauck, R. L. (2012). Growth Factor Supplementation Improves Native and Engineered Meniscus Repair *In Vitro*. *Acta Biomater.* 8 (10), 3687–3694. doi:10.1016/j.actbio.2012.06.005

Kang, S.-W., Sun-Mi, S., Jae-Sun, L., Eung-Seok, L., Kwon-Yong, L., Sang-Guk, P., et al. (2006). Regeneration of Whole Meniscus Using Meniscal Cells and Polymer Scaffolds in a Rabbit Total Meniscectomy Model. *J. Biomed. Mater. Res.* 77A (4), 659–671. doi:10.1002/jbm.a.30579

Kondo, S., Nakagawa, Y., Mizuno, M., Katagiri, K., Tsuji, K., Kiuchi, S., et al. (2019). Transplantation of Aggregates of Autologous Synovial Mesenchymal Stem Cells for Treatment of Cartilage Defects in the Femoral Condyle and the Femoral Groove in Microminipigs. *Am. J. Sports Med.* 47 (10), 2338–2347. doi:10.1177/0363546519859855

Kopeć, K., Wojasiński, M., and Ciach, T. (2020). Superhydrophilic Polyurethane/Polydopamine Nanofibrous Materials Enhancing Cell Adhesion for Application in Tissue Engineering. *Ijms* 21 (18), 6798. doi:10.3390/ijms21186798

Kwon, H., Brown, W. E., Lee, C. A., Wang, D., Paschos, N., Hu, J. C., et al. (2019). Surgical and Tissue Engineering Strategies for Articular Cartilage and Meniscus Repair. *Nat. Rev. Rheumatol.* 15 (9), 550–570. doi:10.1038/s41584-019-0255-1

Li, H., Li, P., Yang, Z., Gao, C., Fu, L., Liao, Z., et al. (2021). Meniscal Regenerative Scaffolds Based on Biopolymers and Polymers: Recent Status and Applications. *Front. Cel Dev. Biol.* 9, 661802. doi:10.3389/fcell.2021.661802

Li, P., Zhang, W., Yu, H., Zheng, L., Yang, L., Liu, G., et al. (2016). Applying Electrospun Gelatin/Poly(lactic Acid-Co-Glycolic Acid) Bilayered Nanofibers to Fabrication of Meniscal Tissue Engineering Scaffold. *J. Nanosci Nanotechnol* 16 (5), 4718–4726. doi:10.1166/jnn.2016.12412

Li, Y., Chen, M., Zhou, W., Gao, S., Luo, X., Peng, L., et al. (2020). Cell-free 3D Wet-Electrospun PCL/silk fibroin/Sr2+ Scaffold Promotes Successful Total Meniscus Regeneration in a Rabbit Model. *Acta Biomater.* 113, 196–209. doi:10.1016/j.actbio.2020.06.017

Lohmander, L. S., Englund, P. M., Dahl, L. L., and Roos, E. M. (2007). The Long-Term Consequence of Anterior Cruciate Ligament and Meniscus Injuries. *Am. J. Sports Med.* 35 (10), 1756–1769. doi:10.1177/0363546507307396

Magaz, A., Roberts, A. D., Faraji, S., Nascimento, T. R. L., Medeiros, E. S., Zhang, W., et al. (2018). Porous, Aligned, and Biomimetic Fibers of Regenerated Silk Fibroin Produced by Solution Blow Spinning. *Biomacromolecules* 19 (12), 4542–4553. doi:10.1021/acs.biomac.8b01233

Makris, E. A., Hadidi, P., and Athanasiou, K. A. (2011). The Knee Meniscus: Structure-Function, Pathophysiology, Current Repair Techniques, and Prospects for Regeneration. *Biomaterials* 32 (30), 7411–7431. doi:10.1016/j.biomaterials.2011.06.037

Marrella, A., Lagazzo, A., Dellacasa, E., Pasquini, C., Finocchio, E., Barberis, F., et al. (2018). 3D Porous Gelatin/PVA Hydrogel as Meniscus Substitute Using Alginate Micro-particles as Porogens. *Polymers* 10 (4), 380. doi:10.3390/polym10040380

Martin, I., Jakob, M., Schäfer, D., Dick, W., Spagnoli, G., and Heberer, M. (2001). Quantitative Analysis of Gene Expression in Human Articular Cartilage from normal and Osteoarthritic Joints. *Osteoarthritis and Cartilage* 9 (2), 112–118. doi:10.1053/joca.2000.0366

Martinek, V., Ueblacker, P., Bräun, K., Nitschke, S., Mannhardt, R., Specht, K., et al. (2006). Second Generation of Meniscus Transplantation: In-Vivo Study with Tissue Engineered Meniscus Replacement. *Arch. Orthop. Trauma Surg.* 126 (4), 228–234. doi:10.1007/s00402-005-0025-1

Medeiros, E. L. G., Braz, A. L., Porto, I. J., Menner, A., Bismarck, A., Boccaccini, A. R., et al. (2016). Porous Bioactive Nanofibers via Cryogenic Solution Blow Spinning and Their Formation into 3D Macroporous Scaffolds. *ACS Biomater. Sci. Eng.* 2 (9), 1442–1449. doi:10.1021/acsbiomaterials.6b00072

Medeiros, E. S., Glenn, G. M., Klamczynski, A. P., Orts, W. J., and Mattoso, L. H. C. (2009). Solution Blow Spinning: A New Method to Produce Micro- and Nanofibers from Polymer Solutions. *J. Appl. Polym. Sci.* 113 (4), 2322–2330. doi:10.1002/app.30275

Milachowski, K. A., Weismeier, K., and Wirth, C. J. (1989). Homologous Meniscus Transplantation. *Int. Orthopaedics* 13 (1), 1–11. doi:10.1007/BF00266715

Molde, J., Steele, J. A. M., Pastino, A. K., Mahat, A., Murthy, N. S., and Kohn, J. (2020). A Step toward Engineering Thick Tissues: Distributing Microfibers within 3D Printed Frames. *J. Biomed. Mater. Res.* 108 (3), 581–591. doi:10.1002/jbm.a.36838

Murphy, C. A., Garg, A. K., Silva-Correia, J., Reis, R. L., Oliveira, J. M., and Collins, M. N. (2019). The Meniscus in Normal and Osteoarthritic Tissues: Facing the Structure Property Challenges and Current Treatment Trends. *Annu. Rev. Biomed. Eng.* 21, 495–521. doi:10.1146/annurev-bioeng-060418-052547

Oda, S., Otsuki, S., Kurokawa, Y., Hoshiyama, Y., Nakajima, M., and Neo, M. (2015). A New Method for Meniscus Repair Using Type I Collagen Scaffold and Infrapatellar Fat Pad. *J. Biomater. Appl.* 29 (10), 1439–1448. doi:10.1177/0885328215568984

Oliveira, J. E., Moraes, E. A., Costa, R. G. F., Afonso, A. S., Mattoso, L. H. C., Orts, W. J., et al. (2011). Nano and Submicrometric Fibers of poly(D,L-lactide) Obtained by Solution Blow Spinning: Process and Solution Variables. *J. Appl. Polym. Sci.* 122 (5), 3396–3405. doi:10.1002/app.34410

Pak, J., Lee, J. H., and Lee, S. H. (2014). Regenerative Repair of Damaged Meniscus with Autologous Adipose Tissue-Derived Stem Cells. *Biomed. Res. Int.* 2014, 1–10. doi:10.1155/2014/436029

Polk, S., Sori, N., Thayer, N., Kemper, N., Maghdouri-White, Y., Bulysheva, A. A., et al. (2018). Pneumatospinning of Collagen Microfibers from Benign Solvents. *Biofabrication* 10 (4), 045004. doi:10.1088/1758-5090/aad7d0

Puetzer, J. L., Koo, E., and Bonassar, L. J. (2015). Induction of Fiber Alignment and Mechanical Anisotropy in Tissue Engineered Menisci with Mechanical Anchoring. *J. Biomech.* 48 (8), 1436–1443. doi:10.1016/j.jbiomech.2015.02.033

Qu, D., Zhu, J. P., Childs, H. R., and Lu, H. H. (2019). Nanofiber-based Transforming Growth Factor-B3 Release Induces Fibrochondrogenic Differentiation of Stem Cells. *Acta Biomater.* 93, 111–122. doi:10.1016/j.actbio.2019.03.019

Qu, F., Holloway, J. L., Esterhai, J. L., Burdick, J. A., and Mauck, R. L. (2017). Programmed Biomolecule Delivery to Enable and Direct Cell Migration for Connective Tissue Repair. *Nat. Commun.* 8 (1), 1780. doi:10.1038/s41467-017-01955-w

Rai, M. F., Brophy, R. H., and Rosen, V. (2020). Molecular Biology of Meniscus Pathology: Lessons Learned from Translational Studies and Mouse Models. *J. Orthop. Res.* 38 (9), 1895–1904. doi:10.1002/jor.24630

Resmi, R., Parvathy, J., John, A., and Joseph, R. (2020). Injectable Self-Crosslinking Hydrogels for Meniscal Repair: A Study with Oxidized Alginate and Gelatin. *Carbohydr. Polym.* 234, 115902. doi:10.1016/j.carbpol.2020.115902

Rodeo, S. A., Monibi, F., Dehghani, B., and Maher, S. (2020). Biological and Mechanical Predictors of Meniscus Function: Basic Science to Clinical Translation. *J. Orthop. Res.* 38 (5), 937–945. doi:10.1002/jor.24552

Rothrauff, B. B., Sasaki, H., Kihara, S., Overholt, K. J., Gottardi, R., Lin, H., et al. (2019). Point-of-Care Procedure for Enhancement of Meniscal Healing in a Goat Model Utilizing Infrapatellar Fat Pad-Derived Stromal Vascular Fraction Cells Seeded in Photocrosslinkable Hydrogel. *Am. J. Sports Med.* 47 (14), 3396–3405. doi:10.1177/0363546519880468

Rueden, C. T., Schindelin, J., Hiner, M. C., DeZonia, B. E., Walter, A. E., Arena, E. T., et al. (2017). ImageJ2: ImageJ for the Next Generation of Scientific Image Data. *BMC Bioinformatics* 18 (1), 529. doi:10.1186/s12859-017-1934-z

Santos, A. M. C., Medeiros, E. L. G., Blaker, J. J., and Medeiros, E. S. (2016). Aqueous Solution Blow Spinning of Poly(vinyl Alcohol) Micro- and Nanofibers. *Mater. Lett.* 176, 122–126. doi:10.1016/j.matlet.2016.04.101

Sasaki, H., Rothrauff, B. B., Alexander, P. G., Lin, H., Gottardi, R., Fu, F. H., et al. (2018). *In Vitro* Repair of Meniscal Radial Tear with Hydrogels Seeded with Adipose Stem Cells and TGF-B3. *Am. J. Sports Med.* 46 (10), 2402–2413. doi:10.1177/0363546518782973

Sekiya, I., Koga, H., Otabe, K., Nakagawa, Y., Katano, H., Ozeki, N., et al. (2019). Additional Use of Synovial Mesenchymal Stem Cell Transplantation Following Surgical Repair of a Complex Degenerative Tear of the Medial Meniscus of the Knee: A Case Report. *Cel Transpl.* 28 (11), 1445–1454. doi:10.1177/0963689719863793

Shimomura, K., Bean, A. C., Lin, H., Nakamura, N., and Tuan, R. S. (2015). *In Vitro* Repair of Meniscal Radial Tear Using Aligned Electrospun Nanofibrous Scaffold. *Tissue Eng. Part A* 21 (13-14), 2066–2075. doi:10.1089/ten.TEA.2014.0549

Singh, R., Ahmed, F., Polley, P., and Giri, J. (2018). Fabrication and Characterization of Core-Shell Nanofibers Using a Next-Generation Airbrush for Biomedical Applications. *ACS Appl. Mater. Inter.* 10 (49), 41924–41934. doi:10.1021/acsami.8b13809

Sinha-Ray, S., Sinha-Ray, S., Yarin, A. L., and Pourdeyhimi, B. (2015). Theoretical and Experimental Investigation of Physical Mechanisms Responsible for Polymer Nanofiber Formation in Solution Blowing. *Polymer* 56, 452–463. doi:10.1016/j.polymer.2014.11.019

Srinivasan, S., Chhatre, S. S., Mabry, J. M., Cohen, R. E., and McKinley, G. H. (2011). Solution Spraying of Poly(methyl Methacrylate) Blends to Fabricate Microtextured, Superoleophobic Surfaces. *Polymer* 52 (14), 3209–3218. doi:10.1016/j.polymer.2011.05.008

Tomecka, E., Wojasinski, M., Jastrzebska, E., Chudy, M., Ciach, T., and Brzozka, Z. (2017). Poly(L -lactic Acid) and Polyurethane Nanofibers Fabricated by Solution Blow Spinning as Potential Substrates for Cardiac Cell Culture. *Mater. Sci. Eng. C* 75, 305–316. doi:10.1016/j.msec.2017.02.055

Tong, J., Xu, X., Wang, H., Zhuang, X., and Zhang, F. (2015). Solution-blown Core-Shell Hydrogel Nanofibers for Bovine Serum Albumin Affinity Adsorption. *RSC Adv.* 5 (101), 83232–83238. doi:10.1039/c5ra19420b

Turman, K., and Diduch, D. (2008). Meniscal Repair - Indications and Techniques. *J. Knee Surg.* 21 (2), 154–162. doi:10.1055/s-0030-1247812

van Schaik, T. J. A., Gaul, F., Dorthé, E. W., Lee, E. E., Grogan, S. P., and D'Lima, D. D. (2021). Development of an *Ex Vivo* Murine Osteochondral Repair Model. *Cartilage* 12 (1), 112–120. doi:10.1177/1947603518809402

Wang, K., Xu, M., Zhu, M., Su, H., Wang, H., Kong, D., et al. (2013). Creation of Macropores in Electrospun Silk Fibroin Scaffolds Using Sacrificial PEO-Microparticles to Enhance Cellular Infiltration. *J. Biomed. Mater. Res.* 101 (12), 3474–3481. doi:10.1002/jbm.a.34656

Wang, X., Ding, Y., Li, H., Mo, X., and Wu, J. (2021). Advances in Electrospun Scaffolds for Meniscus Tissue Engineering and Regeneration. *J. Biomed. Mater. Res.* doi:10.1002/jbm.b.34952

Winkler, P. W., Rothrauff, B. B., Buerba, R. A., Shah, N., Zaffagnini, S., Alexander, P., et al. (2020). Meniscal Substitution, a Developing and Long-Awaited Demand. *J. Exp. Ortop* 7 (1), 55. doi:10.1186/s40634-020-00270-6